Deformable frequency selective surface structure with tuning capability through thermoregulating

Xin Chen,* Jinsong Gao, Chunyi Fang, Nianxi Xu, Yansong Wang and Yang Tang

Key Laboratory of Optical System Advance Manufacturing Technology, Changchun Institute of Optics, Fine Mechanics and Physics, Chinese Academy of Sciences, Changchun 130033, China

*chenxin_19344834@163.com

Abstract: We design and fabricate a deformable frequency selective surface (FSS) structure using shape memory alloys (SMA). The unit cell could "remember" two different geometrical shapes and the shapes convert to each other alternately during heating and cooling, that leads to the drift of resonant frequency. Qualitative analysis by equivalent circuit model and accurate numeric calculation are compared to display the character of the transmission. The measurements show that a tuning range of frequency from 13.07GHz to 16.29GHz is achieved when the morphology of the unit cell changes, making the deformable FSS an attractive choice for tunable filter in different frequency bands with the features of wide tuning range and sharp cut-off.

OCIS codes: (120.2440) Filters; (160.3918) Metamaterials; (260.5740) Resonance; (350.4010) Microwaves; (120.7000) Transmission.

References and links

1. T. K. Wu, *Frequency Selective Surface and Grid Array* (John Wiley and Sons, 1995).
2. B. A. Munk, *Frequency Selective Surfaces: theory and Design* (John Wiley and Sons, 2000).
3. B. A. Munk, *Finite Antenna Arrays and FSS* (John Wiley and Sons, 2003).
4. B. Li and Z. X. Shen, "Angular-stable and polarization-independent frequency selective structure with high selectivity," Appl. Phys. Lett. **103**(17), 171607 (2013).
5. C. Y. Fang, J. S. Gao, and H. Liu, "A novel metamaterial filter with stable passband performance based on frequency selective surface," AIP. Adv. **4**(7), 077114 (2014).
6. N. I. Zheludev, "Applied physics. The road ahead for metamaterials," Science **328**(5978), 582–583 (2010).
7. B. Sanz-Izquierdo, E. A. Parker, and J. C. Batchelor, "Dual-band tunable screen using complementary split ring resonators," IEEE Trans. Antenn. Propag. **58**(11), 3761–3765 (2010).
8. B. Q. Lin, S. B. Qu, C. M. Tong, H. Zhou, H. Y. Zhang, and W. Li, "Varactor-tunable frequency selective surface with embedded bias network," Chin. Phys. B. **22**(9), 094103 (2013).
9. F. Bayatpur and K. Sarabandi, "A tunable metamaterial frequency-selective surface with variable modes of operation," IEEE Trans. Microw. Theory Tech. **57**(6), 1433–1438 (2009).
10. L. Zhang, G. Yang, Q. Wu, and J. Hua, "A novel active frequency selective surface with wideband tuning range for EMC purpose," IEEE Trans. Magn. **48**(11), 4534–4537 (2012).
11. H. Tao, A. C. Strikwerda, K. Fan, W. J. Padilla, X. Zhang, and R. D. Averitt, "Reconfigurable terahertz metamaterials," Phys. Rev. Lett. **103**(14), 147401 (2009).
12. H. Tao, A. C. Strikwerda, K. Fan, W. J. Padilla, X. Zhang, and R. D. Averitt, "MEMS based structurally tunable metamaterials at terahertz frequencies," J. Infrared Milli. Terahz. Waves. **32**(5), 580–595 (2011).
13. H. Kim, Y. Yoo, and J. Lee, "Development of a NiTi actuator using a two-way shape memory effect induced by compressive loading cycles," Sens. Actuators A Phys. **148**(2), 437–442 (2008).
14. C. Lexcellent, S. Leclercq, B. Gabry, and G. Bourbon, "The two way shape memory effect of shape memory alloys: an experimental study and a phenomenological model," Int. J. Plast. **16**(10–11), 1155–1168 (2000).
15. W. Huang, "On the selection of shape memory alloys for actuators," Mater. Des. **23**(1), 11–19 (2002).
16. N. Marcuvitz, *Waveguide Handbook* (Boston Technical Publishers, 1964), pp. 280–285.
17. R. Lahoz and J. A. Puértolas, "Training and two-way shape memory in NiTi alloys: influence on thermal parameters," J. Alloys Compd. **381**(1–2), 130–136 (2004).
18. A. Amengual, E. Cesari, and R. Romero, "On the relationship between temperature and critical stress in the two-way shape memory effect of Cu-Zn-Al single crystals," Scr. Metall. Mater. **32**(8), 1269–1275 (1995).
19. E. Cingolani, M. Ahlers, and M. Sade, "The two way shape memory effect in Cu-Zn-Al single crystals: role of dislocations and stabilazations," Acta Metall. Mater. **43**(6), 2451–2461 (1995).

20. G. F. Xu, "The effect of transformation temperature on dry sliding wearability of CuZnAl shape memory alloys," Res. Stud. Foundry Equip. **23**(6), 20–23 (2001).
21. G. F. Xu, N. C. Si, and Y. X. Li, "Rolling wearabilities of different structural state CuZnAl shape memory alloys," Chin. J. Nonferrous Met. **14**(5), 825–830 (2004).
22. Y. Bellouard, "Shape memory alloys for microsystems: A review from a material research perspective," in *Proceedings of the 7th European Symposium on Martensitic Transformations*, G. Eggeler and G. Kostorz, ed. (Elsevier, 2008), pp. 582–589.
23. M. Koyama, T. Sawaguchi, K. Ogawa, T. Kikuchi, and M. Murakami, "The effects of thermomechanical training treatment on the deformation characteristics of Fe-Mn-Si-Al alloys," Mater. Sci. Eng. A **497**(1–2), 353–357 (2008).
24. D. A. Miller and D. C. Lagoudas, "Influence of cold work and heat treatment on the shape memory effect and plastic strain development of NiTi," Mater. Sci. Eng. A **308**(1–2), 161–175 (2001).
25. X. L. Meng, Y. F. Zheng, W. Cai, and L. C. Zhao, "Two-way shape memory effect of a TiNiHf high temperature shape memory alloy," J. Alloys Compd. **372**(1–2), 180–186 (2004).
26. Y. Liu, Y. Liu, and J. V. Humbeeck, "Two-way shape memory effect developed by martensite deformation in NiTi," Acta Mater. **47**(1), 199–209 (1998).

1. Introduction

Frequency selective surface (FSS) is a well-established paradigm for filtering electromagnetic waves, particularly in the microwave and radio frequency bands [1–5], and is recognized as the foundation of the modern field of metamaterials [6]. It has been used in a number of applications such as telecommunications, antenna design, electromagnetic compatibility, surface wave manipulation and radar cross section (RCS) management. The conventional FSS is only passive printed conductors on a dielectric substrate, the character of the transmission will not change once designed and manufactured, so the research about tunable FSS has received more attentions. A well-known method is to incorporate lumped components into the elements, for instance, a plenty of tunable FSSs have been designed by embedding varactors or PIN diodes in the unit cell for tuning the resonant frequency [7–10]. But the defect of this method is that the performance of the frequency response will be distorted due to the introduction of the bias network which is used for loading the lumped components. Another method is the use of structurally reconfigurable metamaterials [11,12], the tunable resonant response could be realized through mechanically reorienting the unit cells. But the method is awkward to handle because the operating temperature is higher than 350°C.

So the work described in this paper is motivated by the need to provide a convenient solution to realize the tunable FSS without using the lumped components and offer the theoretic support for the experiment. We design and fabricate the prototype using shape memory alloys (SMA), which enables the unit cell to get memory like the organism and remember two geometrical shapes at low-temperature region as well as high-temperature region [13–15]. Utilizing the reversible conversion between the two kinds of shapes through thermoregulating, the proposed FSS could realize the function of tuning for TE polarization. The unit cell originates from the shorted square loop aperture element, the equivalent circuit model to predict the electromagnetic behavior of the FSS at the resonant frequency is studied and the frequency tuning capability is demonstrated by numerical simulation. The measure results verify the design and simulations, opening up myriad opportunities for realizing tunable FSS in different frequency ranges by altering the shape and size of the unit cell.

2. Model and analysis

The original unit cell is composed of a square mesh surrounding an attached square patch through one cylindrical cantilever structure, called shorted square loop aperture element, and the three-dimensional sketch is shown in Fig. 1. T represents the periodic spacing of the unit cell, w is the width of the gap and the length of the cantilever, Φ is the diameter of the cantilever, b is the width of the wire, l is the side length of the patch and t is the thickness of the metal screen. The frequency response can be designed to resonate at the desired frequency for both TE and TM polarization by adjusting the perimeter of the square loop aperture and the dimension of the patch.

#238076 - $15.00 USD Received 15 Apr 2015; revised 4 Jun 2015; accepted 5 Jun 2015; published 11 Jun 2015

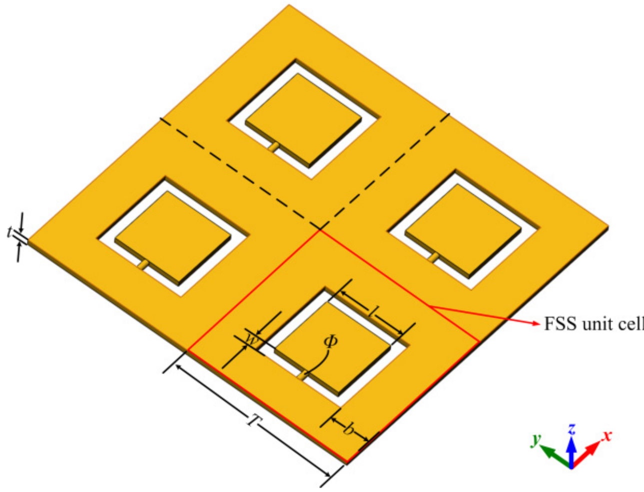

Fig. 1. Three-dimensional sketch of the original unit cell.

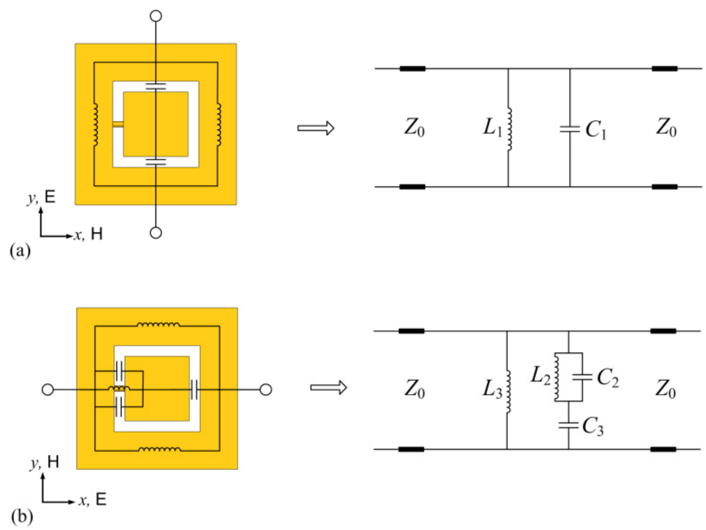

Fig. 2. Equivalent circuit model of the original FSS structure for TE polarization (a) and TM polarization (b).

The resonant behavior of the FSS exposed to the normal incidence in free space environment can be illuminated effectively according to the equivalent circuit model. When the incident electric field is perpendicular to the cantilever structure (TE incidence) as shown in Fig. 2(a), the resonant frequency f_1 is very close to the one of square loop aperture element which has a band-pass performance, because the equivalent circuit model is the same parallel LC circuit shunted across a transmission line. The inductance L_1 is derived from the wires along the vertical direction while the gaps along the horizontal direction represent the total capacitance C_1. Conversely, when the incident electric field is parallel to the cantilever structure (TM incidence) as shown in Fig. 2(b), the FSS structure could be equal to a parallel LC circuit (L_2 and C_2) in series with the capacitance C_3, then in parallel with the inductance L_3. Qualitative analysis from the circuit model implies that there are two resonances in the considerable frequency range. The higher resonant frequency f_2 mainly depends on L_2 and C_2, which could be understood as the cantilever and its surrounding gaps respectively. The lower resonant frequency f_3 is mostly determined by L_3 and C_3, they are derived from the wires along the horizontal direction and the gap on the right side of the unit cell.

The free space impedance Z_0 is 377Ω, the first-order approximation of the capacitance C and the inductance L can be expressed respectively [16]:

$$C_1 = \varepsilon_0 \frac{l}{\pi} \log\left[\csc\left(\frac{\pi w}{2l}\right)\right], \tag{1}$$

$$L_1 = \mu_0 \frac{T}{4\pi} \log\left[\csc\left(\frac{\pi b}{2T}\right)\right], \tag{2}$$

$$C_2 = \varepsilon_0 \frac{2(l-\Phi)}{\pi} \log\left\{\csc\left[\frac{\pi w}{2(l-\Phi)}\right]\right\}, \tag{3}$$

$$L_2 = \mu_0 \frac{w}{2\pi} \log\left[\csc\left(\frac{\pi \Phi}{2w}\right)\right], \tag{4}$$

$$C_3 = \varepsilon_0 \frac{2l}{\pi} \log\left[\csc\left(\frac{\pi w}{2l}\right)\right], \tag{5}$$

$$L_3 = \mu_0 \frac{T}{4\pi} \log\left[\csc\left(\frac{\pi b}{2T}\right)\right]. \tag{6}$$

ε_0 and μ_0 represent permittivity of vacuum and permeability of vacuum respectively. We can see that the capacitance value is determined by the effective side length of the patch facing to the adjacent wires and the width of the gaps, if the position of metallic patch varies, the capacitance value will change regularly and generate new resonant status.

Inspired by the qualitative analysis and discussions above, a notion to design a tunable FSS structure is brought out and shown in Fig. 3. It approximates that the cantilever structure rotates at an angle of θ, changing the effective side length of the patch facing to the adjacent wires and the width of the gaps. That means C_1, C_2 and C_3 are the functions of the angle of θ and become adjustable.

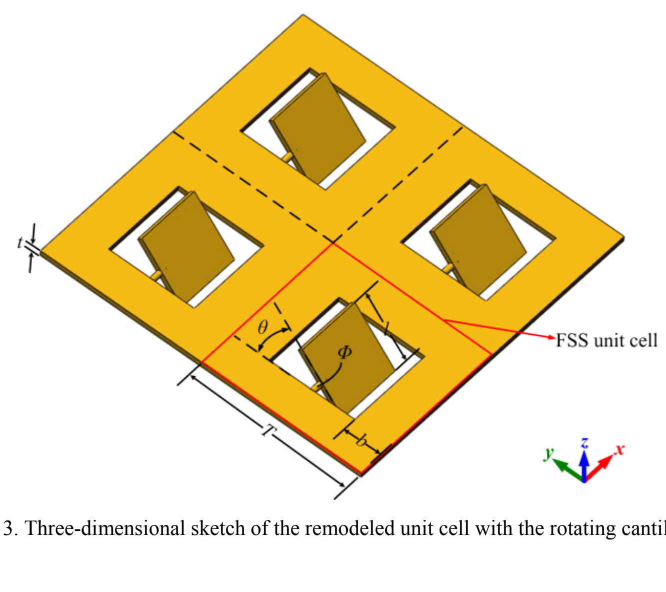

Fig. 3. Three-dimensional sketch of the remodeled unit cell with the rotating cantilever.

As shown in Fig. 4(a) for TE polarization, though the shape of the unit cell is remodeled, the corresponding equivalent circuit model is still similar to the prior one except the capacitance C_1 is replaced by C_θ which would be adjustable if we can control the value of θ as we expect. The effective side length of the patch stabilizes but the width of the gaps expands rapidly when the value of θ enhances, which leads to a decrease of the corresponding capacitance C_θ and an increase of the resonant frequency. We conclude that owing to the tuning capability of the capacitance C_θ, the resonant frequency can be lowered or heightened effectively.

C_θ' and C_θ'' vary at the same time when the value of θ increases or decreases according to Fig. 4(b) for TM polarization. But only the effective side length of the patch changes slowly due to the thickness of the metal screen, whereas the width of the gaps remains stable all the time, thus the variation of the capacitance either C_θ' or C_θ'' is slower than C_θ, and the drift of each resonant frequency is inconspicuous.

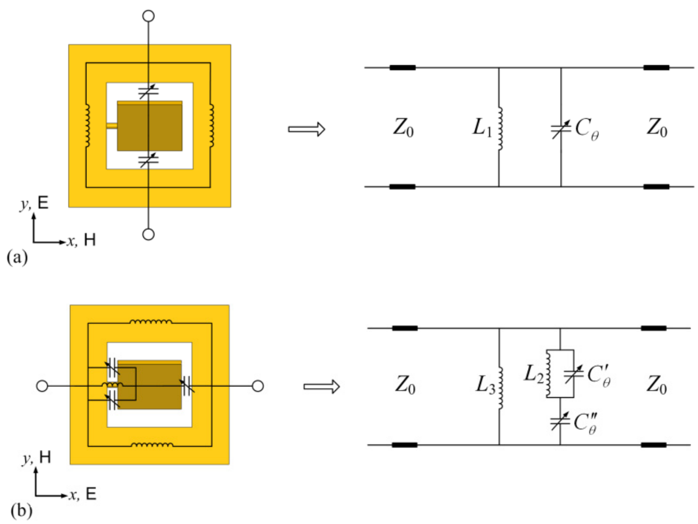

Fig. 4. Equivalent circuit model of the remodeled FSS structure for TE polarization (a) and TM polarization (b).

In order to verify the correctness of the idea, full-wave analysis of the structure is performed by using CST software, the transmission spectrum of the filter is determined by solving the Maxwell equations in the finite-integral time-domain method and we compare it with the consequence from equivalent circuit model. The dimensions of each unit cell are as follows: T = 15mm, w = 1mm, Φ = 0.5mm, b = 3.5mm, l = 6mm and t = 0.5mm. When the value of θ is assumed to be different, the frequency response for both polarizations under normal incidence are obtained in Fig. 5, the results of full-wave analysis and equivalent circuit model are observed to be in good agreement with each other. When the value of θ is 0°, the characteristic parameters are as follows: C_1 = 0.301pF, L_1 = 0.508nH, C_2 = 0.436pF, L_2 = 0.321nH, C_3 = 0.602pF and L_3 = 0.508nH. According to the resonant frequency and bandwidth of the transmission spectrum, the capacitance values are also synthesized respectively by adjusting the values of C in the circuit model using ADS circuit simulation until the S-parameters of the circuit model are the same with the results from CST software when the value of θ varies.

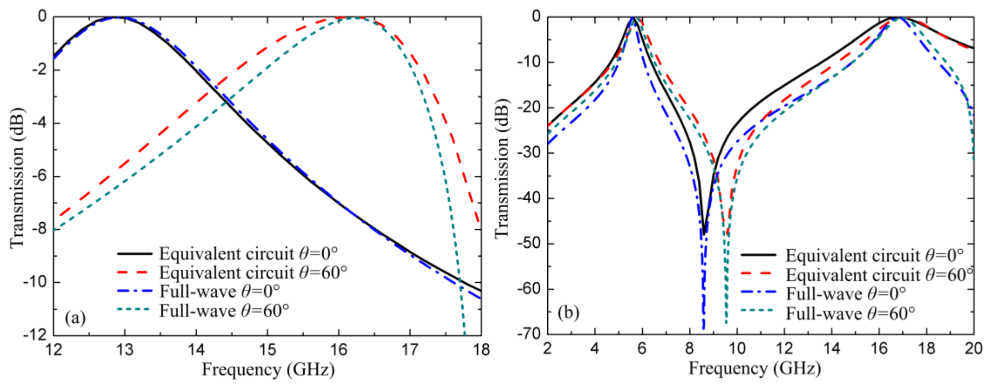

Fig. 5. Frequency response obtained from full-wave simulations and predicted by equivalent circuit model of the remodeled FSS structure with different values of θ for TE polarization (a) and TM polarization (b).

From Fig. 5(a) we find that a wide tuning range from 12.92GHz to 16.22GHz is achieved by changing the value of θ from 0° to 60° for TE polarization, because the capacitance value is diminished from 0.301pF to 0.195pF, a strong resonance can be produced at a higher frequency. For TM polarization, both of the two resonant frequencies are nearly invariable though the value of θ changes dramatically as shown in Fig. 5(b). The characteristic parameters of the remodeled FSS are also summarized in Table 1 and Table 2 for both polarizations when the value of θ is different.

Table 1. The characteristic parameters of the remodeled FSS with different values of θ for TE polarization

θ (°)	f_1 GHz	T_1 dB	C_θ pF
0	12.92	–0.023	0.301
20	13.78	–0.021	0.262
40	15.14	–0.026	0.216
60	16.22	–0.043	0.195

Table 2. The characteristic parameters of the remodeled FSS with different values of θ for TM polarization

θ (°)	f_2 GHz	T_2 dB	C_θ' pF	f_3 GHz	T_3 dB	C_θ'' pF
0	16.78	–0.059	0.436	5.58	–0.148	0.602
20	16.86	–0.081	0.412	5.64	–0.129	0.598
40	16.94	–0.095	0.405	5.72	–0.101	0.590
60	16.96	–0.083	0.397	5.76	–0.081	0.581

The transmission performances of the FSS structure at various incident angles for both polarizations are also provided in Fig. 6 when the value of θ is different. As shown in Fig. 6(a), the transmission spectrum suffers from an unwanted variation of resonant frequency and the grating lobe appears when the incident angle α varies from 0° to 40°, it has sensitivity to the incident angle for TE polarization; though a similar situation exists with the higher resonant frequency in Fig. 6(b) for TM polarization, there is a positive result that the lower resonant frequency is stable when the incident angle α increases from 0° to 40°.

#238076 - $15.00 USD Received 15 Apr 2015; revised 4 Jun 2015; accepted 5 Jun 2015; published 11 Jun 2015

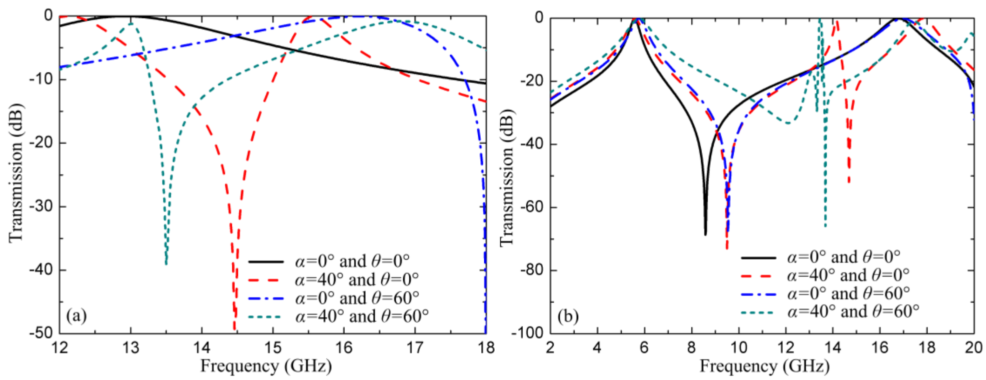

Fig. 6. Frequency response of the remodeled FSS structure at various incident angles with different values of θ for TE polarization (a) and TM polarization (b)

3. Fabrication and testing

In order to change the shape of the original unit cell properly, one simple and effective method is that we machine the prototype using SMA, a type of reversible and spontaneous shape change of temperature-sensing material which could exhibit two stable shapes instead of one: a high-temperature shape in the austenite phase and a low-temperature shape in the martensite phase [17–19]. The single crystal with a nominal composition of copper(69.62wt.%), zinc(25.7wt.%), aluminum(3.81wt.%), nickel(0.8wt.%), lanthanum(0.04wt.%) and cerium(0.04wt.%) is prepared by induction melting at 1250°C under an argon atmosphere, after homogenizing at 850°C for 24h the ingot is hot-rolled and cold-rolled into a plate with the thickness of 0.5mm [20,21]. Then we obtain the sample with the dimension of 300mm × 300mm × 0.5mm by cutting from the plate and realize the original unit cell aforementioned with machining operation [22,23], except the cantilever structure is a cube with the width of 0.5mm instead of the cylinder for easy processing.

By using the method mentioned in [20], we obtain the following values of characteristic transformation temperatures: M_s = 64°C, M_f = 52°C, A_s = 58°C, A_f = 70°C. M_s, M_f, A_s, and A_f denote martensitic transformation start temperature, martensitic transformation finish temperature, reverse martensitic transformation start and finish temperature, respectively.

The sample is trained in rotating the patches according to the procedure known as training [24–26]. Heating the sample by hot air until it is in the phase of high temperature then rotate the patches slowly and enable the value of θ increase to about 65°, afterwards maintain the configuration unchangeable with stress as cooling it to room temperature by cold air; when reheating the sample to the phase of high temperature, the cantilever rotates spontaneously in the opposite direction until the value of θ is about 10°. And repeat the aforementioned procedure 15 times.

In such a way the prototype can recover a shape not only on heating but also during cooling. The unit cell has its own memory about ambient temperature and could achieve a reversible and macroscopic shape change: upon cooling the patch rises and lays down on heating. When the FSS is heated to a temperature higher than 70°C by hot air, the value of θ is about 10° as shown in Fig. 7(a); after the temperature drops to 52°C below, the value of θ is about 60° as shown in Fig. 7(b).

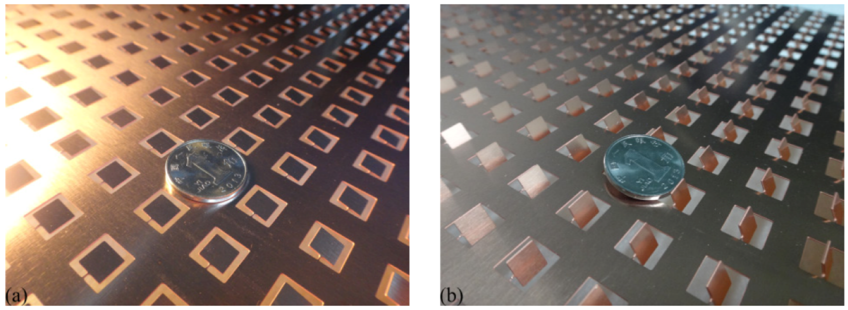

Fig. 7. The working states of the sample at high-temperature region (a) and low-temperature region (b).

For characterizing the behavior of the prototype, an experiment is carried out in Ku-band and the measurement system comprises an Agilent N5244A vector network analyzer, a pair of lens antenna, a bearing bracket, an electric heater and a hot air gun. We use the electric heater and the hot air gun to heat the sample in order to guarantee its temperature is high enough, the testing for both polarizations is achieved by rotating the sample 90° under normal incidence.

4. Results and discussion

After a cycle of heating and cooling, a smooth tuning range of frequency is achieved from 13.07GHz to 16.29GHz during the temperature of the sample drops as shown in Fig. 8(a) for TE polarization, and the frequency response remains unchanged for TM polarization as shown in Fig. 8(b), the transmission peaks are nearly 0dB. The results of measurements and simulations are similar with each other in the same working states, except that there is a little difference at the frequency deviating from the resonant frequency, that may be attributed to the fabrication tolerance and the inconsistency of rotation angle produced in the training process, in addition, the cylindrical cantilever structure is replaced by the cube. Nevertheless, this experiment can be used to verify the accuracy of our prediction and simulations in the previous sections.

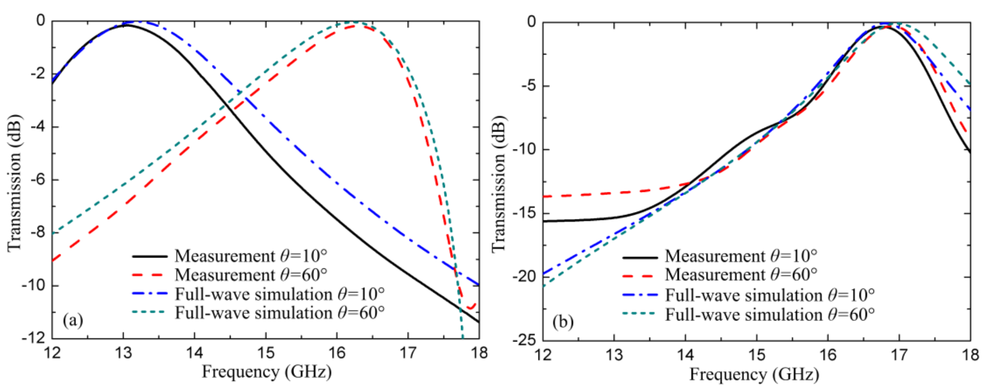

Fig. 8. Comparison between simulation and measurement in two working states for TE polarization (a) and TM polarization (b).

To better understand the influence of the deformation process of the unit cell on the frequency response, we can gain some insight into the variation of electric energy density distribution on the FSS pattern at the resonant frequencies under normal incidence when the value of θ is different. As shown in Fig. 9(a), at 12.92GHz we find the maximum on the edges of the patch and wires along the horizontal direction because of the strong coupling between them when the value of θ is 0°, by contrast, the vertical direction do not contribute to the resonance. And the electric energy density decreases visibly when the cantilever structure

#238076 - $15.00 USD Received 15 Apr 2015; revised 4 Jun 2015; accepted 5 Jun 2015; published 11 Jun 2015

rotates from 0° to 60°, it predicts that by changing the relative position of the patches and wires, we can have a major influence on the electric energy density distribution and change the frequency response of the filter. And it is indeed the case as show in Fig. 9(b), the location of the maximal electric energy density at 16.22GHz is similar to the case before, but the change of magnitude has the opposite tendency, it increases when the cantilever structure rotates from 0° to 60°. That means the resonant frequency is corresponding to the emergence of the maximal electric energy density and if we can control the distribution of electric energy density on the FSS pattern, the filter will realize the function of tuning, which confirms that the resonant frequency drifts distinctly when the morphology of the unit cell alters for TE polarization.

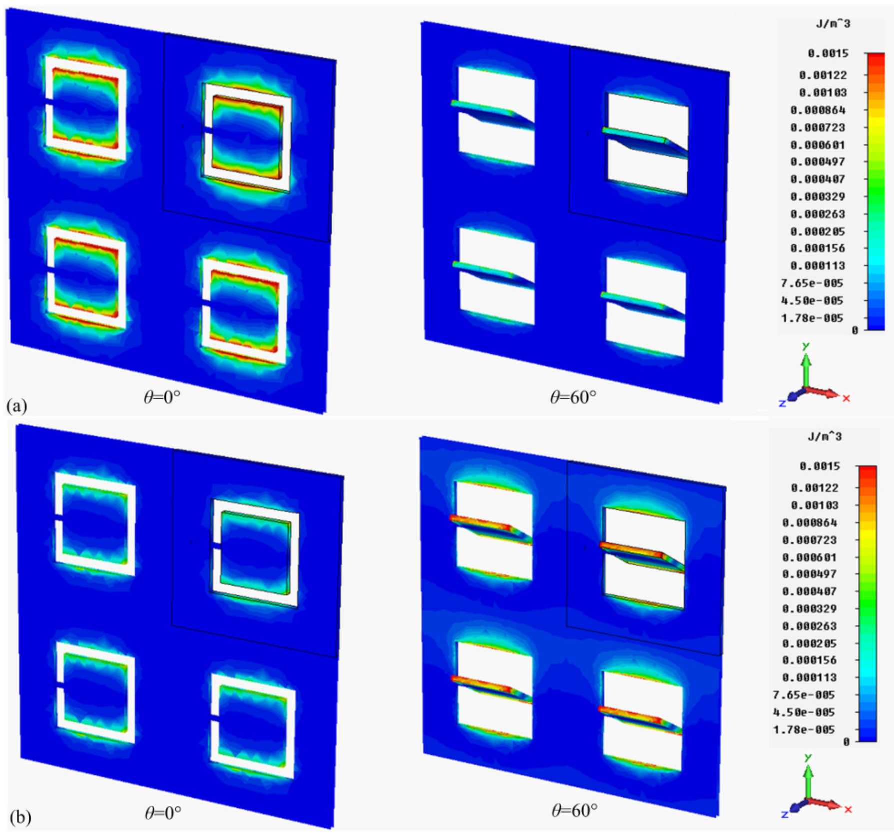

Fig. 9. Distributions of electric energy density on the FSS pattern for TE polarization under normal incidence with different values of θ at 12.92GHz (a) and 16.22GHz (b).

Figure 10 shows the distributions of electric energy density on the FSS pattern at 5.58GHz and 16.78GHz which correspond to the lower and higher resonant frequency respectively for TM polarization. It can be found that the electric resonances occur in the right side slot and the left corners of the unit cell. No matter how much is the value of θ, the electric energy is almost invariable and distributes in the same areas of the pattern at respective resonant frequency. It implies that the resonant frequencies will be stationary, which is consistent with the analysis of the equivalent circuit model.

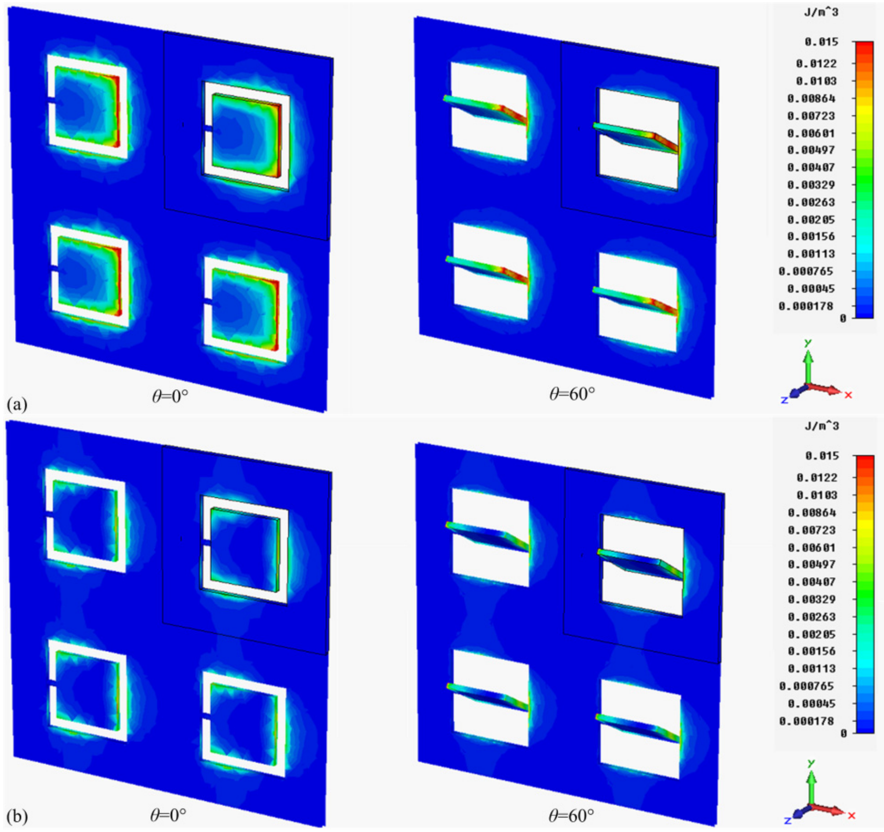

Fig. 10. Distributions of electric energy density on the FSS pattern for TM polarization under normal incidence with different values of θ at 5.68GHz (a) and 16.89GHz (b).

5. Conclusion

In this paper, we present a novel tunable FSS which works for TE polarization is made of SMA. The frequency tuning capability is achieved because the structure of the unit cell could convert between two different shapes as we expect. The behavior of resonance is analyzed step by step by using the equivalent circuit model and the change rules of electric energy density distribution on the FSS pattern are obtained from CST. In order to validate the proposal, one prototype is fabricated and measured at high-temperature region and low-temperature region, the results indicate that the resonant frequency drifts from 13.07GHz to 16.29GHz when the cantilever structure rotates from 10° to 60° and the transmission performances are close to 0dB at the resonant frequency, which verifies the design and simulations.

A deformable FSS structure at other wave bands could also be designed utilizing some similar appearances and the sharper cut-off could be achieved if the thickness of the metal screen increases. Compared with the previous tunable FSSs, our proposed one has more excellent performance without using lumped components, giving us a new design method for the tunable spatial filters and a valuable reference for the application in engineering development.

Acknowledgments

This work is supported by National Natural Science Foundation of China (Grant Nos. 61401424).